Available online at www.sciencedirect.com
SCIENCE DIRECT®
Journal of Sound and Vibration 290 (2006) 910–927
JOURNAL OF SOUND AND VIBRATION
www.elsevier.com/locate/jsvi

Overcritical high-speed rotor systems, full annular rub and accident

O. Grāpis[a], V. Tamužs[b,*], N.-G. Ohlson[c], J. Andersons[b]

[a]*Riga Technical University, Kalku 1, Riga LV-1658, Latvia*
[b]*Institute of Polymer Mechanics, Aizkraukles 23, Riga LV-1006, Latvia*
[c]*Alfa Laval Tumba AB, SE-14780 Tumba, Sweden*

Received 16 February 2003; received in revised form 22 February 2005; accepted 29 April 2005
Available online 19 August 2005

Abstract

Transient response of an overcritical high-speed rotor is considered. A rapid increase of unbalance initiates a series of rotor–stator collisions succeeded by full annular rub during which a very high dynamic load can develop, exceeding by several times that due to separate collisions. The main reasons leading to such a potentially catastrophic response are highlighted.

1. Introduction

A specific malfunction of rotor operation known as full annular rub, characterized by a continuous contact between rotor and stator, has been considered in a number of studies. In Ref. [1] Muszynska notes: ''The most important is the self-excited backward precession of the shaft, known as ''dry whip''. In this mode the shaft rolls while sliding against the seal in the direction opposite to the direction of rotation and maintains contact with the seal. High normal forces and corresponding friction forces at the contacting surfaces may lead to extremely severe damage in merely a few seconds. Most often seals are damaged or destroyed.'' (Here the seal constitutes a stationary surface joined to the stator, with which the rotating part contacts.) Muszynska and

*Corresponding author. Tel.: +371 7543306; fax: +371 7820467.
E-mail address: tamuzs@pmi.lv (V. Tamužs).

0022-460X/$ - see front matter © 2005 Elsevier Ltd. All rights reserved.
doi:10.1016/j.jsv.2005.04.031

Nomenclature

c_x, c_y direction cosines of vector $\boldsymbol{\rho}$ in frame of reference O_axy

$d = 25\,\mathrm{N\,s/m}$ total dissipative force characteristic of both supports

$d_t = 1 \times 10^4\,\mathrm{N\,s/m}$ internal friction parameter of the contact zone material

$e_x = 0.15 \times 10^{-3}\,\mathrm{m}$ mass centre deflection from rotor geometrical centre O

$e_{x1} = k_u e_x$ mass centre deflection from rotor geometrical centre O after the separation of mass m_u

F_τ sliding friction force during impact or continuous rub

F_n impact (or continuous rub) force in radial direction

F_{nx}, F_{ny}, $F_{\tau x}$, $F_{\tau y}$ projections of the forces F_n, F_τ in frame of reference O_axy

F_{in} radial inertia force of rotor translatory motion during rotor fast rolling

$g = 9.81\,\mathrm{m/s^2}$ acceleration due to gravity

$I_C = 9 \times 10^{-3}\,\mathrm{kg\,m^2}$ rotor moment of inertia with respect to its mass centre C

I_{Cn} rotor moment of inertia with respect to centre C after mass separation

$I_{C1} = 8.91 \times 10^{-3}\,\mathrm{kg\,m^2}$ rotor moment of inertia with respect to its new mass centre C_1 after mass m_u separation

$k = 20 \times 10^3\,\mathrm{N/m}$ the total radial stiffness of both rotor supports

$k_t = 8 \times 10^8\,\mathrm{N/m}$ contact spring stiffness

$k_u = 3$ coefficient of deflection e_x increase

L_0 rotor angular momentum about mass centre C before mass separation

L_1 total angular momentum of mass m_u and rotor about centre C upon mass separation

$M_{\mathrm{mot}} = 0.3\,\mathrm{N\,m}$ or 0 driving torque applied to rotor by engine

M_{imp} impact (or continuous contact) force moment about centre O_a

$m = 5\,\mathrm{kg}$ rotor mass

$m_u = 0.0248\,\mathrm{kg}$ mass that separates from rotor rim

$f = \dot{q}_3/2\pi\,\mathrm{Hz}$ rotation velocity of the rotor

$f_{\max} = 150\,\mathrm{Hz} = 943\,\mathrm{rad/s}$ rotation velocity in stable operating regime of the rotor

$f_{\mathrm{rol}} = 770\,\mathrm{Hz}$ rotation velocity of "fast rolling" without slipping

$Q_i, i = 1 \ldots 3$ generalized forces

$q_i, i = 1 \ldots 3$ generalized coordinates

$r = 0.06\,\mathrm{m}$ rotor radius

$r_a = 0.063\,\mathrm{m}$ radius of stator contact ring

T rotor kinetic energy

T_{tra} kinetic energy of rotor curvilinear translatory motion during fast rolling

$t_1 = 29.1\,\mathrm{s}$ instant of mass m_u separation

v_{Cx}, v_{Cy} absolute velocity projections of rotor mass centre C in fame of reference O_axy

$v_{\mathrm{DC}} = 56.7\,\mathrm{m/s}$ relative velocity of mass m_u with respect to mass centre C at the separation instant

v_K absolute velocity of rotor rim point K

v_{K/O_a} relative velocity of K to O_a caused by rotation of O_axy system

v_{Kn}, $v_{K\tau}$ velocity v_K projections in fame of reference $Kn\tau$

v_{Kx}, v_{Ky} velocity v_K projections in fame of reference O_axy

v_{rx}, v_{ry} components of the relative velocity of K in the rotating coordinate system O_axy

Greek letters

Δ radial deformation of material during impact or continuous contact

$\Delta_{vy} = 0.283\,\mathrm{m/s}$ additional (instant) mass centre velocity change along O_ay-axis

$\mu = 0.08$, 0.2 or 0.3 Coulomb friction coefficient between rotor and stator contact ring

ρ rotor geometrical centre displacement from rotation axis O_az_a

Goldman [2] present the results of numerical and experimental studies for an unbalanced rotor in regimes in which contact between rotor and stator occurs. In stationary regimes, harmonic and subharmonic as well as chaotic forms of vibration are present. A regime when rotor is in continuous contact with stator and the direction of rotor centre rotation is opposite to the shaft rotation direction is also observed. Choy et al. [3] consider a rotor with 4dof. The effect of rotor and casing inertia parameters, contact surface friction, and nonlinearity of turbine blade radial and lateral stiffness on dynamics of the system is studied. It is found that rotor motion may transfer from rigid to chaotic bouncing and then to full rub. Dai et al. [4,5] compare experimental data and modelling results for a rotor with four degrees of freedom. A situation is considered when contact of the rotor with a stationary surface takes place in the low critical frequency zone of the rotor due to the action of external harmonic electromagnetic excitation force with correspondingly low frequency. If the amplitude of the excitation force exceeds a certain level, then partial as well as full rubbing behaviour is observed. The aim is to determine the relation between contact zone stiffness and the conditions for occurrence of full rubbing. Choi [6] presents test and modelling results for rotor–stator contact situations. The rotor mass is about 1 kg, the natural frequency 23 Hz, and the rotation speed varies up to 1200 rpm (20 Hz). Backward rolling and backward slipping regimes are observed. It is established that the friction coefficient between the rotor and stator is the major parameter governing the occurrence of these regimes.

In the present paper, a specific case is considered when full annular rub sets in owing to a sudden increase of unbalance of a high-speed rotor operating at overcritical speed. In this case, particularly large dynamic loads arise which can cause catastrophic consequences within a few hundredths of a second. The process resembles explosion. The development of the process in time and its physical essentials are analysed. The dynamics of rotor total kinetic energy variation are considered. Kinetic energy is partially dissipated by friction and partially transferred to the kinetic energy of translatory motion, which causes huge dynamic loads in the contact zone. The main reasons for this behaviour are indicated.

2. Model

2.1. Differential equations of motion

A simple model is considered: an axisymmetric rotor with symmetrically arranged supports shown schematically in Fig. 1(a). The axis of rotation is horizontal. The rotor consists of a flywheel mounted on a rigid shaft. The rotor has only a static unbalance; its dynamic unbalance is taken equal to zero. Hence, the rotor is restricted to in-plane motion and the problem reduces to rotor motion analysis in the vertical plane of symmetry $O_a x_a y_a$, Fig. 1(b).

The bearing supports are linearly elastic, the transmitted force being proportional to the radial displacement of the rotor axis; the total stiffness of both supports is denoted by k. Vibration dampers are connected in parallel, the damping force being proportional to the radial velocity of the rotor axis; the damping constant of both supports is denoted by d.

The rotor motion is composed of rotation and translation. Two coordinate systems are therefore introduced, a fixed frame of reference $O_a x_a y_a$, the origin of which, O_a, coincides with the geometrical centre O of the rotor in static equilibrium, Fig. 1(a), and a rotating frame of reference

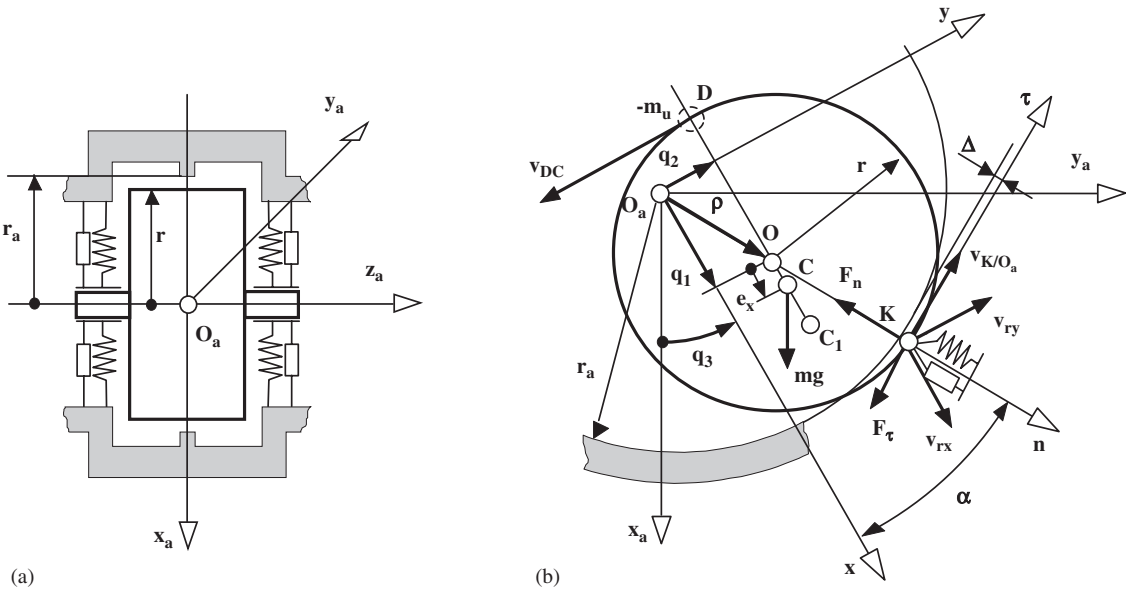

Fig. 1. Vertical cross-sections of rotor in static equilibrium (a) and rotor in motion (b).

O_axy, Fig. 1(b). Three generalized coordinates determine the rotor position, namely coordinates q_1 and q_2 for translatory motion, and coordinate q_3 for rotation. A static unbalance is created by displacing the mass centre C in the radial direction a distance e_x. As previously mentioned, the stator is symmetrically arranged around the balanced rotor. Contact between rotor and stator is assumed to occur in the plane of symmetry, as indicated in Fig. 1(a).

The projections of the absolute velocity of rotor mass centre C in the frame of reference O_axy are

$$v_{Cx} = \dot{q}_1 - \dot{q}_3 q_2 \quad v_{Cy} = \dot{q}_2 + \dot{q}_3(q_1 + e_x). \tag{1}$$

Then the kinetic energy is given by

$$T = \frac{1}{2} m\left(v_{Cx}^2 + v_{Cy}^2\right) + \frac{1}{2} I_C \dot{q}_3^2. \tag{2}$$

By applying the Lagrange equation

$$\frac{\mathrm{d}}{\mathrm{d}t}\left(\frac{\partial T}{\partial \dot{q}_i}\right) - \frac{\partial T}{\partial q_i} = Q_i, \quad i = 1,\ 2,\ 3,$$

we obtain

$$\begin{aligned}
&m\ddot{q}_1 - mq_2\ddot{q}_3 - 2m\dot{q}_3\dot{q}_2 - m\dot{q}_3^2(q_1 + e_x) = Q_1,\\
&m\ddot{q}_2 + m(q_1 + e_x)\ddot{q}_3 + 2m\dot{q}_3\dot{q}_1 - m\dot{q}_3^2 q_2 = Q_2,\\
&\left\{I_C + m\left|(q_1 + e_x)^2 + q_2^2\right|\right\}\ddot{q}_3 - mq_2\ddot{q}_1\\
&\quad + m(q_1 + e_x)\ddot{q}_2 + 2m\dot{q}_1\dot{q}_3(q_1 + e_x) + 2m\dot{q}_2\dot{q}_3 q_2 = Q_3.
\end{aligned} \tag{3}$$

The generalized forces are determined by the following expressions:

$$\begin{aligned} Q_1 &= -d(\dot{q}_1 - \dot{q}_3 q_2) - kq_1 + F_{nx} + F_{\tau x}, \\ Q_2 &= -d(\dot{q}_2 + \dot{q}_3 q_1) - kq_2 + F_{ny} + F_{\tau y}, \\ Q_3 &= d(\dot{q}_1 - \dot{q}_3 q_2) q_2 - d(\dot{q}_2 + \dot{q}_3 q_1) q_1 \\ &\quad - mg\left[(q_1 + e_x)\sin q_3 + q_2 \cos q_3\right] + M_{\text{mot}} + M_{\text{imp}}. \end{aligned} \tag{4}$$

Here M_{mot} is the torque exerted by the engine on the rotor. Forces F_n, F_τ shown in Fig. 1(b) and their moment, M_{imp}, about the centre O_a arise during rotor–stator contact. In the absence of contact, these forces and their moment vanish.

2.2. Effect of increase of unbalance

In normal overcritical operation, the rotor self-centres around its mass centre, a recognized advantage during overcritical rotation. Rotor–stator contact may occur due to lack of sufficient clearance between parts, in particular after a rapid increase of rotor unbalance. The latter may be caused by a redistribution of mass within the rotor, or by an unsymmetrical loss of mass from the rotor. The latter case is considered here, namely, a mass loss of m_u on radius r, from the opposite side of the rotor relative to the initial unbalance, at point D, Fig. 1(b). (The mass may separate from any point on the rotor rim; the location is not crucial for transient rotor dynamics. The specific case described above is chosen to simplify the analysis; note also that it leads to the largest unbalance increase for a given m_u). The mass m_u separates from rotor due to centrifugal forces and causes increase of deflection e_x by a factor of k_u, i.e. $e_{x1} = k_u e_x$. The lost mass m_u and the resulting deflection are interrelated as follows:

$$m_u = m\frac{e_{x1} - e_x}{r + e_{x1}}. \tag{5}$$

In the stable self-centring service regime, the relative motion of the rotor in $O_a xy$ frame of reference has ceased and rotor mass centre C almost coincides with centre O_a.

In the following, alterations in Eqs. (3) and (4) after separation of mass m_u are derived. At the instant of mass separation, the velocity of mass m_u is equal to that of the rotor rim point D. Therefore upon mass separation, the total angular momentum about centre C of both objects, the separated particle (i.e. material point) and the rotor, is equal to that of the rotor before separation. This means that the angular velocity of the plane motion of the rotor, $\dot{q}_3$, does not change either. It can be also proved as follows. The angular momentum L_0 about mass centre C before mass separation is

$$L_0 = I_C \dot{q}_3. \tag{6}$$

The relative velocity of the separated mass m_u with respect to centre C is

$$v_{\text{DC}} = \dot{q}_3(r + e_x). \tag{7}$$

The moment of inertia of the rotor, I_{Cn}, about centre C is no longer central after mass loss and is given by

$$I_{Cn} = I_C - m_u(r + e_x)^2. \tag{8}$$

If one assumes that the angular velocity of the plane motion has also changed and equals $\dot{q}_{3n}$ then, upon mass separation, the total angular momentum L_1 of the material point and rotor about centre C becomes

$$L_1 = m_u\dot{q}_3(r+e_x)^2 + \left[I_C - m_u(r+e_x)^2\right]\dot{q}_{3n}. \tag{9}$$

Due to conservation of the angular momentum, $L_0 = L_1$; it follows from Eqs. (6), (9) that

$$I_C\dot{q}_3 = m_u\dot{q}_3(r+e_x)^2 + \left[I_C - m_u(r+e_x)^2\right]\dot{q}_{3n}. \tag{10}$$

It is concluded from Eq. (10) that $\dot{q}_{3n} = \dot{q}_3$, as it was stated above.

The central moment of inertia I_{C1} about the new mass centre C_1 is determined using the relation

$$I_{Cn} = I_{C1} + (m-m_u)(e_{x1}-e_x)^2. \tag{11}$$

Taking into account Eq. (8) we obtain

$$I_{C1} = I_C - m_u(r+e_x)^2 - (m-m_u)(e_{x1}-e_x)^2. \tag{12}$$

The total momentum of the separated mass and the rotor upon separation also has to be equal to that of the rotor before separation; therefore by projecting momentum change vectors on the O_ay axis we obtain

$$-m_u v_{\mathrm{DC}} + (m-m_u)\Delta_{vy} = 0, \tag{13}$$

where Δ_{vy} is the additional change in rotor mass centre velocity along O_ay-axis. Accounting for Eq. (7) we obtain

$$\Delta_{vy} = \frac{m_u\dot{q}_3(r+e_x)}{m-m_u}. \tag{14}$$

One can also verify that the total kinetic energy is not changed by the separation of mass m_u.

Consequently, differential equations (3) and relations (1), (2), (4) still apply upon mass separation with the following modifications: e_x, I_C, m have to be substituted by e_{x1}, I_{C1}, $m_1 = m - m_u$ correspondingly, and the instantaneous alteration of generalized velocity $\dot{q}_2$ by Δ_{vy} has to be taken into account.

2.3. Contact forces

Consider the forces acting at the rotor–stator contact. The contact is modelled by introducing a spring at a contact point with a parallel dashpot modelling material internal friction (Fig. 1b). It is assumed that the contact spring is linear and the internal friction force in the material is proportional to deformation rate, the factor of proportionality being d_t. Since the deformation of the rotor and the stator ring in the radial direction is likely to be very small, we make the simplifying assumption that the rotor radius r remains constant during contact. The Coulomb friction force at the contact point is taken proportional to the normal pressure at this point, the factor of proportionality being μ.

In order to determine the forces acting at the rim point K, the absolute velocity (i.e. the velocity with respect to stator) of this point, $\mathbf{v}_K$, has to be established. The velocity can be expressed as

$$\mathbf{v}_K = \mathbf{v}_{K/O_a} + \mathbf{v}_{rx} + \mathbf{v}_{ry}, \tag{15}$$

where $\mathbf{v}_{K/O_a}$ is the relative velocity of point K with respect to O_a caused by rotation of O_axy system,

$$v_{K/O_a} = \dot{q}_3(\rho + r) = \dot{q}_3(r_a + \Delta) \tag{16}$$

and $\mathbf{v}_{rx}$, $\mathbf{v}_{ry}$ are the components of the relative velocity of K in the rotating coordinate system O_axy. Motion of the rotor in the rotating frame of reference O_axy is translatory, therefore all points on the rotor have the same velocity of relative motion

$$v_{rx} = \dot{q}_1, \quad v_{ry} = \dot{q}_2. \tag{17}$$

Noting that the magnitude and direction cosines of the displacement vector $\boldsymbol{\rho}$ of the rotor geometrical centre O are given by

$$\rho = \sqrt{q_1^2 + q_2^2}, \quad c_x = \cos\alpha = \frac{q_1}{\rho}, \quad c_y = \sin\alpha = \frac{q_2}{\rho}, \tag{18}$$

the projections of $\mathbf{v}_K$ on axes Kn, $K\tau$ and O_ax, O_ay are

$$\begin{aligned} v_{Kn} &= \dot{q}_2 c_y + \dot{q}_1 c_x, & v_{Kx} &= \dot{q}_1 - (r_a + \Delta)\dot{q}_3 c_y, \\ v_{K\tau} &= \dot{q}_3(r_a + \Delta) + \dot{q}_2 c_x - \dot{q}_1 c_y, & v_{Ky} &= \dot{q}_2 + (r_a + \Delta)\dot{q}_3 c_x. \end{aligned} \tag{19}$$

The radial deformation and its rate are

$$\Delta = \rho + r - r_a, \quad \dot{\Delta} = v_{Kn}. \tag{20}$$

If $\Delta \leqslant 0$ then the rotor does not touch the stator, and consequently impact forces are zero. During contact, the impact force component F_n in the radial direction and its projections on the axes O_ax, O_ay are determined by the relations:

$$F_n = -k_t\Delta - d_t\dot{\Delta}, \quad F_{nx} = F_n c_x, \quad F_{ny} = F_n c_y. \tag{21}$$

When $F_n \geqslant 0$, contact is lost. This condition reflects the fact that interaction between rotor and stator contact ring can end in the final phase of impact already before condition $\Delta = 0$ is fulfilled, if elastic and internal friction forces acting in opposite directions are equal.

The magnitude of the Coulomb friction force is

$$F_\tau = \mu F_n. \tag{22}$$

Vector $\mathbf{F}_\tau$ is directed opposite to the velocity component $\mathbf{v}_{K\tau}$ at the contact point. This condition is fulfilled if their scalar product is negative:

$$\mathbf{F}_\tau \cdot \mathbf{v}_K = F_{\tau x} \cdot v_{Kx} + F_{\tau y} \cdot v_{Ky} < 0. \tag{23}$$

Then

$$F_{\tau x} = F_\tau c_y = -\mu F_{ny}, \quad F_{\tau y} = -F_\tau c_x = \mu F_{nx}. \tag{24}$$

If condition (23) is violated for the given signs of friction force projections, then signs in (24) have to be reversed: $F_{\tau x} = \mu F_{ny}$, $F_{\tau y} = -\mu F_{nx}$.

The moment of the Coulomb friction force F_τ about centre O_a is

$$M_{\text{imp}} = F_{\tau y}(r_a + \Delta)c_x - F_{\tau x}(r_a + \Delta)c_y. \tag{25}$$

3. Numerical analysis

The numerical values of the rotor system parameters are given in the Nomenclature. The rotor is powered by a constant driving torque $M_{\text{mot}} = 0.3\,\text{N m}$. Fig. 2 shows the variation of the generalized coordinates q_1, q_2 and displacement $\rho = \sqrt{q_1^2 + q_2^2}$ of the rotor geometrical centre O during the first 6.5 s of the startup process, when the critical angular velocity zone is being passed, the eigenfrequency being 10 Hz. After 28.3 s the design rotation velocity (150 Hz) is reached and driving torque M_{mot} is switched off. Upon completion of the transient process the relative rotor motion in the rotating frame of reference O_axy ceases because velocities $\dot{q}_1 = \dot{q}_2 = 0$. (Consequently, centre O_a is the instantaneous velocity centre for the plane motion of the rotor.) Self-centring has occurred and rotor mass centre C is located at a distance of 0.7 μm from the rotation axis, i.e. centre O_a.

The driving torque is switched off before the sudden unbalance increase in order to clarify the physical essence of the evolution of dynamic loads and the mechanical energy of the system without the contribution of M_{mot}.

The initial mass centre deflection from the rotor geometrical centre O is assumed as $e_x = 0.15 \times 10^{-3}\,\text{m}$ (which corresponds to an unbalance $me_x = 75\,\text{g cm}$). The rotor unbalance increase factor is taken as $k_u = 3$. Then the rotor mass loss according to Eq. (5) is $m_u = 24.8\,\text{g}$, i.e. 0.5% of rotor mass. Consequently, unbalance of rotor attains the value of $(m - m_u)k_ue_x = 223.9\,\text{g cm}$. Central moment of inertia decreases by 1% and becomes $I_{C1} = 8.91 \times 10^{-3}\,\text{kg m}^2$ as given by Eq. (12).

At the end of the transient process, at time instant $t_1 = 29.1\,\text{s}$, mass m_u separates from the rotor with relative velocity $v_{\text{DC}} = 56.7\,\text{m/s}$ with respect to mass centre C. Simultaneously, an instantaneous additional change by $\Delta_{vy} = 0.283\,\text{m/s}$ of velocity $\dot{q}_2$ and hence also rotor mass centre velocity along the O_ay axis occurs. Rotor collisions with the contact ring begin.

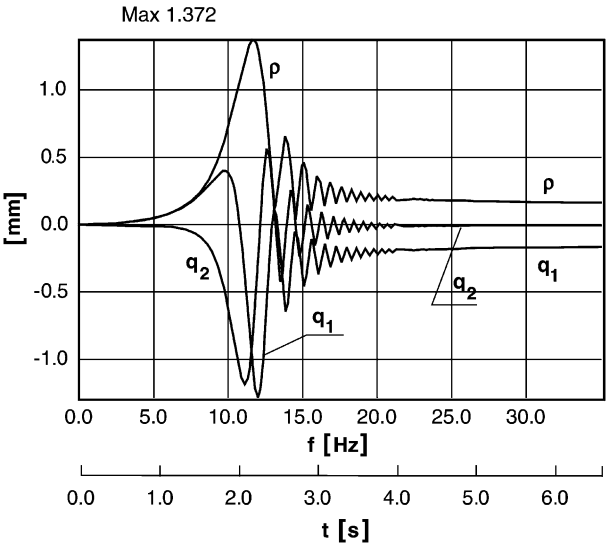

Fig. 2. Rotor startup process.

The radial component of rotor impact force F_n and rotor angular velocity f as functions of time are shown in Figs. 3 and 4 correspondingly. Three cases with comparatively high, intermediate, and low values of Coulomb friction coefficient μ are compared here in order to illustrate the effect of sliding friction on rotor dynamics.

For $\mu = 0.08$, a series of separate collisions of about 0.15 s total duration is initiated by unbalance increase. Then a continuous rotor–stator contact sets in, during which rotor rolling with simultaneous sliding takes place at a very low force F_n, and the rotation velocity gradually decreases. The horizontal parts of the graphs of the rotation velocity, Fig. 4, correspond to contact-free rotor motion, whereas the steep parts reflect the decrease of rotation velocity during each impact.

For $\mu = 0.3$ continuous stator–rotor contact occurs already after a few collisions due to the higher friction force. In a very short time (0.023 s) rotor velocity drops from 150 to 45 Hz and at

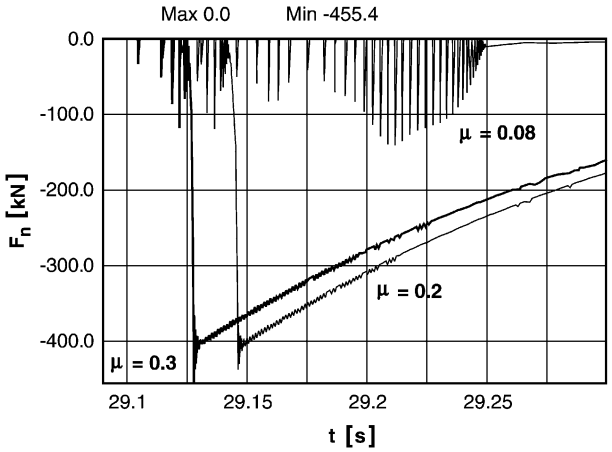

Fig. 3. Radial component F_n of impact force for $\mu = 0.08$, 0.2 and $\mu = 0.3$.

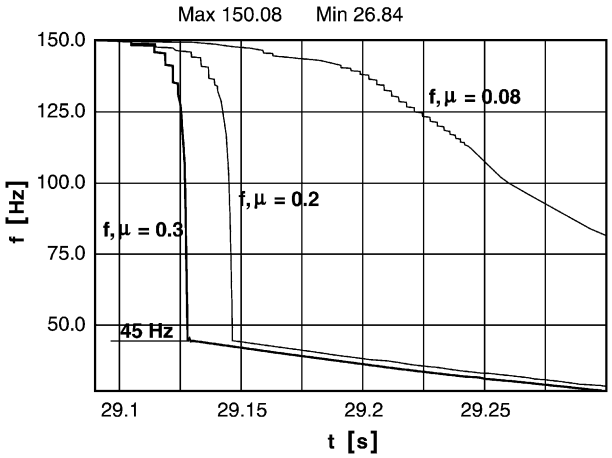

Fig. 4. Variation of rotation velocity $f = \dot{q}_3/2\pi$ of the rotor for $\mu = 0.08$, 0.2 and $\mu = 0.3$.

the same time the radial component of contact force F_n increases to 400–450 kN, thus exceeding by several times the radial impact forces of the separate collisions.

Fig. 5 shows the variation of radial force F_n during several collisions, and the subsequent rapid increase of the force. The variation of rotor kinetic energy in the same time interval is shown in Fig. 6.

The series of collisions is succeeded by rotor rolling along the contact ring accompanied by slipping but without distinct impacts. When force F_n reaches its maximum value, slipping stops, the rotor engages in rolling without slipping, and very rapid relative motion of rotor geometrical centre O in rotating frame of reference O_axy begins (Fig. 7). The trajectory of rotor geometrical centre O in fixed frame of reference $O_ax_ay_a$ is shown in Fig. 8 for $\mu = 0.3$ and in Fig. 9 for $\mu = 0.08$.

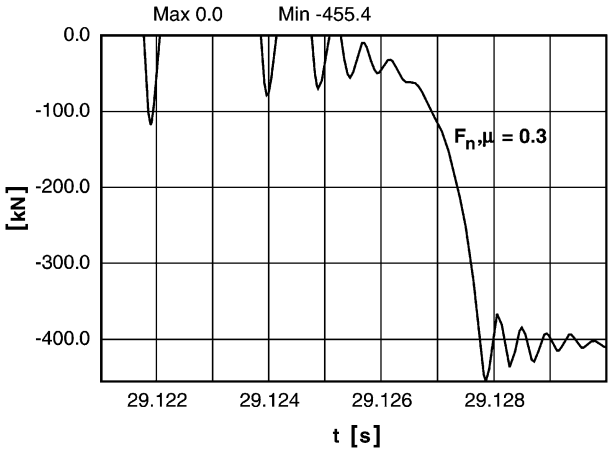

Fig. 5. Impact force F_n during transition from separate collisions to continuous rotor–stator contact.

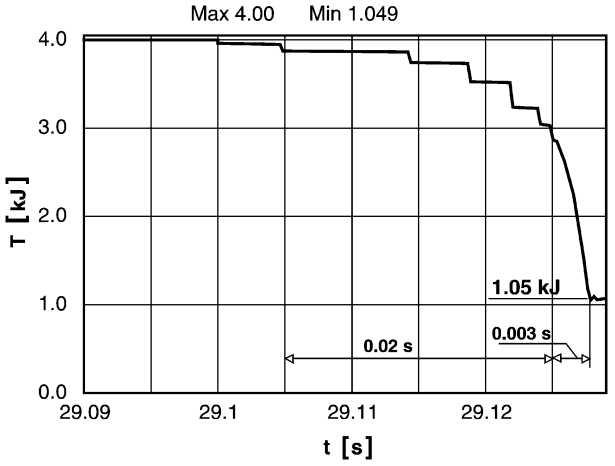

Fig. 6. Variation of rotor kinetic energy T ($\mu = 0.3$).

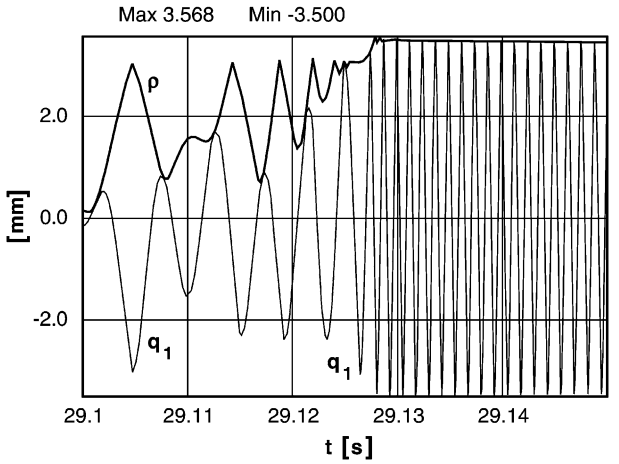

Fig. 7. Variation of the generalized coordinate q_1 in rotating axes O_axy and variation of radius vector $\boldsymbol{\rho}$.

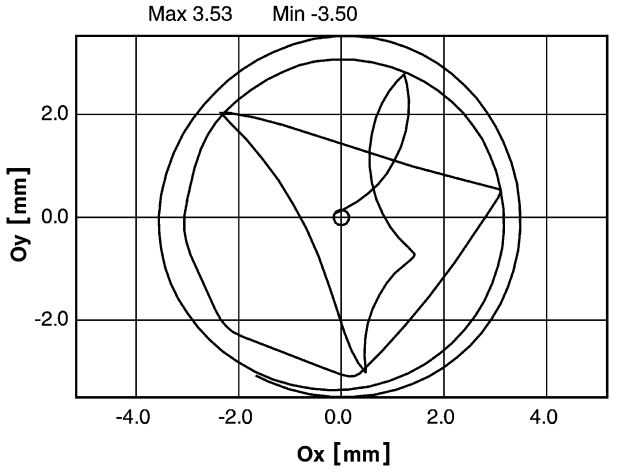

Fig. 8. Trajectory of rotor geometrical centre O in fixed frame of reference $O_ax_ay_a$ during time interval 29.0–29.13 s in the case of $\mu = 0.3$.

The generalized coordinate q_1 in the rotating frame of reference (Fig. 7) varies sinusoidally with the frequency of ≈ 770 Hz and slowly decreasing amplitude $\rho \approx 3.5$ mm. Such a full annular rub regime may be characterised as "fast rolling". The situation is similar to a planetary transmission mechanism when at a low rotor velocity of $f = \dot{q}_3/2\pi = 45$ Hz (Fig. 4) point K (i.e. the contact point of the rotor and the stator ring) moves along the stator ring with very large rotation velocity f_{rol} in the direction opposite to rotor rotation. The rotation of rotor geometrical centre O about centre O_a has the same velocity f_{rol}. Rotation velocity f_{rol} depends on the difference between rolling radius and rotor radius (Fig. 10):

$$f_{\text{rol}} = \frac{\dot{q}_3}{2\pi}\frac{r}{(r_a + \Delta) - r} = \frac{\dot{q}_3}{2\pi}\frac{r}{\rho} = 771.4 \text{ Hz}, \tag{26}$$

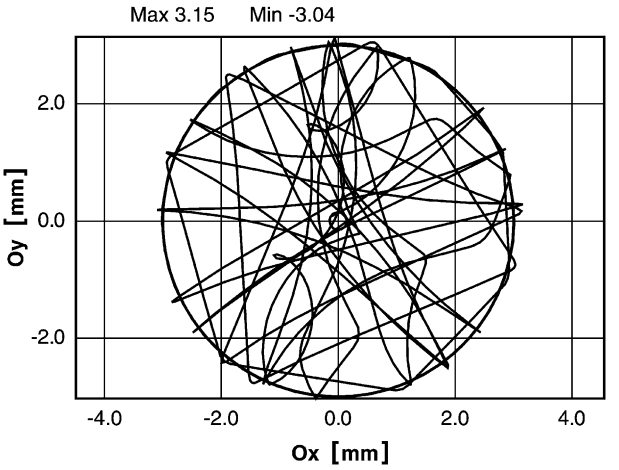

Fig. 9. Trajectory of rotor geometrical centre O in fixed frame of reference $O_a x_a y_a$ during time interval 29.0–29.35 s in the case of $\mu = 0.08$.

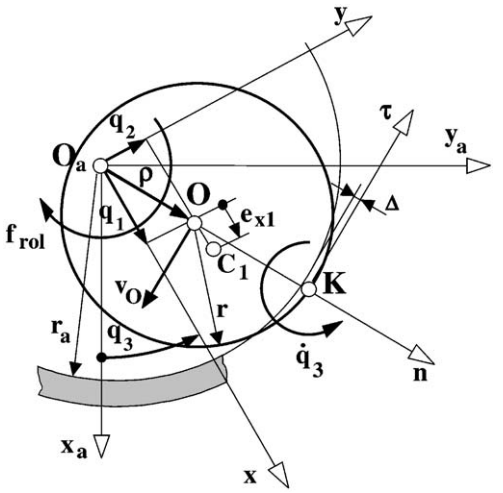

Fig. 10. Scheme of velocities for rotor rolling along the contact ring without slipping.

that also corresponds to the estimated vibration frequency of coordinate q_1 as seen in Fig. 7. The fast rolling causes very large radial force F_n.

The relative motion of the rotor in rotating frame of reference $O_a xy$ is curvilinear translatory motion, therefore all rotor points have the same velocity and acceleration. Trajectories of the points are similar, mutually displaced helices with gradually decreasing radius vector $\boldsymbol{\rho}$. The trajectories are very close to circular with radius $\rho \approx 3.5$ mm in the beginning of the fast rolling process. Let us estimate the radial inertia force F_{in} and kinetic energy T_{tra} due to this translatory motion. Accounting for rotor point velocities in translatory motion $v_{C1} = v_O = 2\pi f_{\text{rol}} \rho =$

16.9 m/s (assuming $f_{\mathrm{rol}} = 770$ Hz, as obtained using the graph in Fig. 7), we obtain

$$T_{\mathrm{tra}} = m_1\left(2\pi f_{\mathrm{rol}}\rho\right)^2 \Big/ 2 = 713.3\ J,$$
$$F_{\mathrm{in}} = m_1\left(2\pi f_{\mathrm{rol}}\right)^2\rho = 407.6\ \mathrm{kN}. \tag{27}$$

The kinetic energy of the rotor before separation of mass m_u is $T = 4000$ J (Fig. 6). At the instant of mass separation, $t_1 = 29.1$ s, the variation of kinetic energy is negligible. Then rotor collisions with stator begin. During collisions, within approximately 0.02 s, the kinetic energy is reduced by about 1000 J by friction forces acting in the contact zone. After that the continuous rotor-stator contact sets in—rotation with slipping. In this regime during about 0.003 s sliding friction forces further reduce the kinetic energy by 1950 J. At the onset of fast rolling without slipping, the remaining kinetic energy of the rotor is only $T = 1050$ J (Fig. 6), i.e. 25% of the initial value. This kinetic energy is composed of the energy of rotor translatory motion $T_{\mathrm{tra}} = 713.3$ J and kinetic energy of rotation (with rotation velocity $f = \dot{q}_3/2\pi \approx 45$ Hz). Consequently, the major part of the remaining kinetic energy has been rapidly transferred from rotational to translatory form. The inertia force of translatory motion, F_{in}, agrees with the values of radial reaction force F_n shown in Figs. 3 and 5.

Note that large dynamic loads develop only at rotor–stator contact zone. The load on the bearings is due to elastic and dissipative forces, and its level is moderate. During the fast rolling of the rotor, the elastic force per bearing is $\rho k/2 = 35$ N. The load per bearing due to dissipative forces is $v_O d/2 = 212$ N, where the velocity of the rotor geometrical centre O (Fig. 10) is $v_O = 2\pi f_{\mathrm{rol}}\rho = 16.9$ m/s.

In the following, the effect of the contact spring stiffness variation on rotor dynamics is considered. The changes in dynamic response are also evaluated when collisions begin at lower rotor velocity f (i.e. lower than the operating velocity $f_{\max}$). Fig. 11 shows the variation of the radial component F_n of impact force for $\mu = 0.3$ and three values of the stiffness, namely k_t, $2k_t$ and $0.5k_t$. Such a large variation of stiffness has only a minor effect on the collision process.

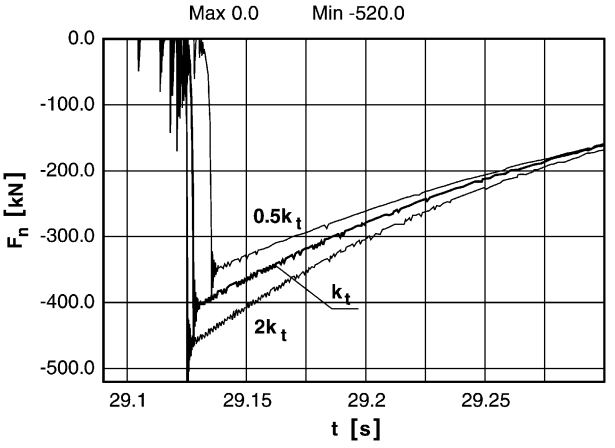

Fig. 11. Contact spring stiffness effect on the variation of the radial component F_n of the impact force. Modelling results for stiffness $k_t = 8 \times 10^8$ N/m, $2k_t$ and $0.5k_t$ are compared.

A nonlinear contact zone stiffness characterization would of course be more realistic. But it appears acceptable to linearize the contact zone response because the collision process is of short duration and therefore only the work of the elastic forces during impact is important. It should also be noted that variation of the internal friction parameter d_t of the contact zone material has a very limited effect on the modelled collision process.

The transient dynamics when the mass m_u separates at rotation velocity f below operating velocity $f_{\max} = 150\,\text{Hz}$ is shown in Figs. 12–17 (at $\mu = 0.3$ and $k_t = 8 \times 10^8\,\text{N/m}$). For $f = 100\,\text{Hz}$ (Fig. 12), the collision process resembles that of $f_{\max} = 150\,\text{Hz}$ case shown in Fig. 3, but the maximum value of the magnitude of force F_n is reduced from 455 to 237 kN. For $f = 75\,\text{Hz}$ (Fig. 13), this force is further reduced to 136 kN. Furthermore, if mass m_u separates at $t_1 = 9.4\,\text{s}$ when rotation velocity $f = 49.8\,\text{Hz}$ (Fig. 14), the rotor does not touch the contact ring during transient process because the gap between the stator contact ring and the rotor rim exceeds the maximum displacement of the rotor geometrical centre. A short transient process is initiated at $t_1 = 9.4\,\text{s}$ that leads to the new self-centring position of the rotor. The initial part of the transient process is shown in Fig. 15, and the rotor geometrical centre trajectory during time interval 9.3–9.8 s is plotted in Fig. 16. Mass separation within the rotor critical angular velocity zone (at $t_1 = 2.2\,\text{s}, f = 11.8\,\text{Hz}$) also does not cause collisions, Fig. 17.

The onset of the fast rolling regime is governed primarily by rotor support stiffness, rotation velocity, Coulomb friction coefficient between rotor and stator contact ring, the gap between them, and the magnitude of the sudden unbalance increase. The development of rotor/stator rubbing is also affected by such parameters as contact zone stiffness, rotor mass and inertia moment, rotor and contact ring dimensions, dissipative characteristics. The effect of the system parameters is interrelated. For more compliant rotor supports, smaller rapid unbalance increase would be necessary for initiating rotor–stator contact. At larger rotation velocity, rotor inertia forces at the instant of unbalance increase would be larger. This interplay of system parameters can be characterized by the ratio of maximum rotation velocity and critical velocity. The critical angular velocity is determined by rotor mass and support stiffness. More compliant rotor

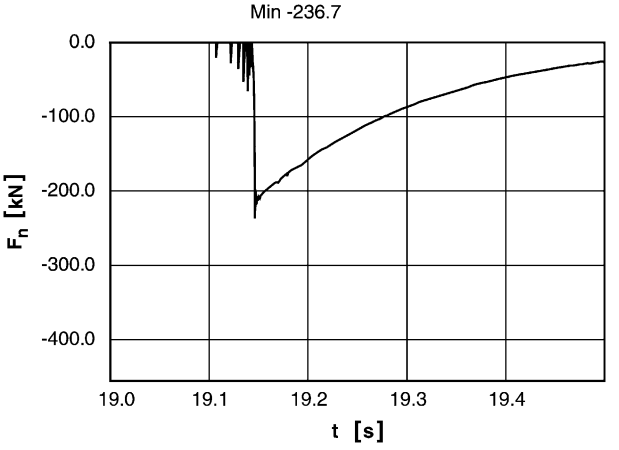

Fig. 12. Radial component F_n of impact force if mass m_u separates at $t_1 = 19.1\,\text{s}$ when rotation velocity $f = 100\,\text{Hz}$. The maximum value of the magnitude of F_n is 237 kN.

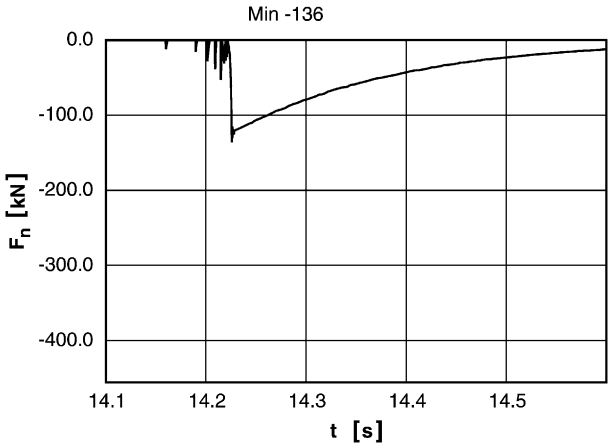

Fig. 13. Radial component F_n of impact force if mass m_u separates at $t_1 = 14.15$ s when rotation velocity $f = 75$ Hz. The maximum value of the magnitude of F_n is 136 kN.

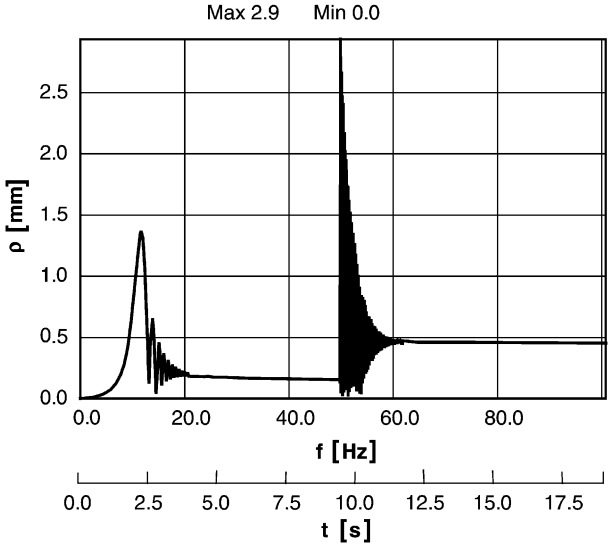

Fig. 14. Variation of the rotor geometrical centre displacement ρ if mass m_u separates at $t_1 = 9.4$ s when rotation velocity $f = 49.8$ Hz. Rotor does not touch the contact ring during transient process leading to the new self-centring position of the rotor.

supports at larger rotor mass lead to lower critical velocity. It follows from the modelling results that higher rotation velocity at the instant of mass loss translates into higher likelihood for fast rolling regime onset and higher forces in the rotor/stator contact zone.

The model analysed above, which assumes linear elasticity in the contact region, is somewhat artificial. The high radial load at contact point K would cause plastic deformation within the contact zone in an engineering application. Heat development due to friction may also cause

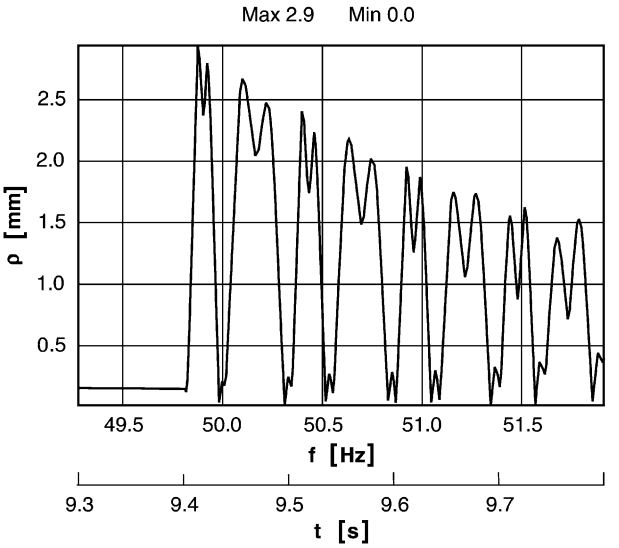

Fig. 15. Rotor geometrical centre displacement ρ. The initial part of the transient process of Fig. 14 corresponding to time interval 9.3–9.8 s.

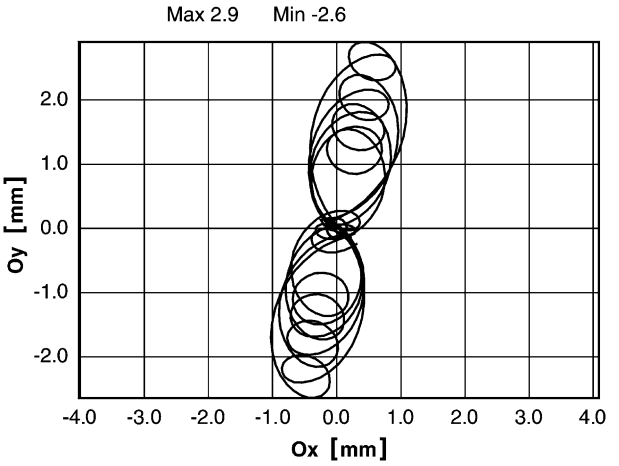

Fig. 16. Trajectory of rotor geometrical centre O in fixed frame of reference $O_a x_a y_a$ during time interval 9.3–9.8 s of the transient process shown in Fig. 15.

degradation. The rapid progress of the impact process with large energy dissipation and huge dynamic load is crucial for the safety of rotors. The aim of the reported numerical analysis is confined to revealing the principal behaviour of the system, including the possibility of a dangerous accident.

Runge–Kutta fourth-order numerical integration method was applied in the numerical analysis. The integration step in startup process modelling was chosen as 1×10^{-4} s. Thus 67 integration steps were performed during one revolution at rotation velocity $f_{\max} = 150$ Hz. The collision

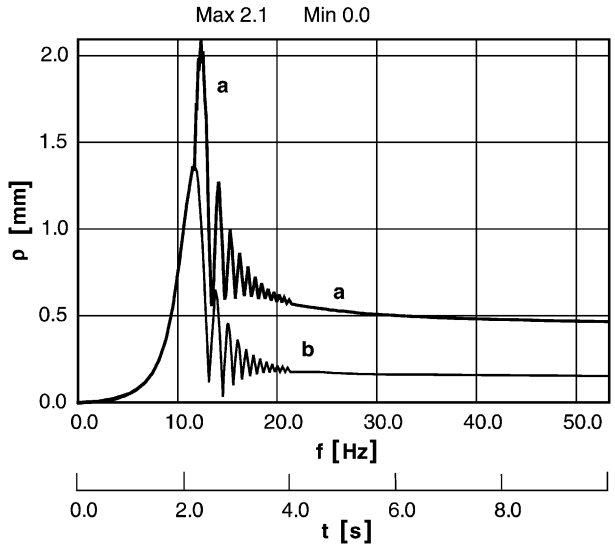

Fig. 17. Variation of the rotor geometrical centre displacement ρ in the critical velocity zone of the rotor. Graph a—mass m_u separates at $t_1 = 2.2$ s when rotation velocity $f = 11.8$ Hz. Graph b—transient process in the absence of mass separation.

process was modelled using integration step of 5×10^{-6} s. Since the duration of a collision varies between 1×10^{-4} and 3×10^{-4} s, 25–60 integration steps were performed during each collision. Note that during fast rolling the rotation velocity of rotor geometrical centre O is 770 Hz and period 1.3×10^{-3} s. Consequently, the integration step used in collision modelling is acceptable also for the fast rolling process.

4. Results

Very high contact forces with ensuing possible catastrophic failure may occur in rotor systems subjected to rapid increase of unbalance. The stepwise increase initiates a series of separate collisions of short duration succeeded by a continuous rotor–stator contact, during which rotor rolling along the contact ring with simultaneous sliding takes place, followed further by fast rolling without slipping. The development of this process upon the first collision is very rapid. During few hundredths of a second (0.023 s for the modelled rotor system), about 75% of rotor kinetic energy is dissipated by the friction forces in the rotor–stator contact zone. At the same time the angular velocity of the rotor drops significantly (~3 times); most of the remaining kinetic energy is transferred to the kinetic energy of translatory motion. Simultaneously with the angular velocity decrease, the radial component of the rotor–stator contact force increases dramatically (modelled rotor with only 5 kg mass develops radial force of ~400 kN), exceeding by several times the radial force developed in the separate collisions. Following the rapid drop of angular velocity, the rotor starts rolling along the contact ring without sliding. The contact point and the large radial force exerted at this point move round the stator ring in the direction opposite to that of

rotor rotation with very high rotation velocity (770 Hz for the modelled system) exceeding by several times the operating rotation velocity of the rotor (150 Hz for the modelled system).

Under such dynamic loads, plastic deformation can arise in the contact zone and the stator can be destroyed. The process resembles explosion due to its very rapid progress and sudden huge dynamic load.

The main reasons that can lead to such an accident are as follows:

- high angular velocity of the rotor at the instant of rapid increase of the unbalance (if the rotor velocity is not high enough, rotor–stator contact does not lead to an accident because the rotor can slide along the contact surface without fast rolling);
- very compliant rotor supports that lead to a large difference between the angular velocity in normal operation and the critical angular velocity of the system;
- small clearance between the rotor and the stator contact ring;
- high sliding friction coefficient between the rotor and the contact ring.

References

[1] A. Muszynska, Rotor-to-stationary element rub-related vibration phenomena in rotating machinery—literature survey, *The Shock and Vibration Digest* 21 (1989) 3–11.

[2] A. Muszynska, P. Goldman, Chaotic responses of unbalanced rotor/bearing/stator systems with looseness or rubs, *Chaos, Solitons & Fractals* 5 (1995) 1683–1704.

[3] F.K. Choy, J. Padovan, J.C. Yu, Full rubs, bouncing and quasi chaotic orbits in rotating equipment, *Journal of the Franklin Institute* 327 (1990) 25–47.

[4] X. Dai, Z. Jin, X. Zhang, Dynamic behavior of the full rotor/stop rubbing: numerical simulation and experimental verification, *Journal of Sound and Vibration* 251 (2002) 807–822.

[5] X. Dai, X. Zhang, X. Jin, The partial and full rubbing of a flywheel rotor-bearing-stop system, *International Journal of Mechanical Sciences* 43 (2001) 505–519.

[6] Y.S. Choi, Investigation on the whirling motion of full annular rotor rub, *Journal of Sound and Vibration* 258 (2002) 191–198.